Optimization of Uniform Amplitude Periodic Linear Phased Arrays for Grating Lobe Reduction

Aslan, Yanki; Onat, Nehir Berk

DOI
10.23919/EuCAP53622.2022.9769377

Publication date
2022

Document Version
Final published version

Published in
2022 16th European Conference on Antennas and Propagation (EuCAP)

Optimization of Uniform Amplitude Periodic Linear Phased Arrays for Grating Lobe Reduction

Yanki Aslan[1], Nehir Berk Onat[2]
Microwave Sensing, Signals and Systems Group, Department of Microelectronics,
Faculty of Electrical Engineering, Mathematics, and Computer Science,
Delft University of Technology, Delft, The Netherlands
{[1]Y.Aslan, [2]N.B.Onat}@tudelft.nl

***Abstract*—The optimization of mode excitation coefficients in linear periodic arrays of multi-mode antenna elements is studied for grating lobe reduction. A novel beamforming architecture is proposed with a new optimization problem based on equi-amplitude element excitations for optimal power efficiency. The capabilities of the proposed synthesis approach on suppressing the grating lobe for wide scan angles, and on maintaining the peak gain at the steering angle are analyzed. A 16-element 0.7-wavelength spaced array of dual-mode circular patch antenna elements is used for demonstration purposes. It is shown that a good performance trade-off is achieved when the excitation amplitude of the high order mode is restricted to a sufficiently large value. The ratio of the peak gain outside the main lobe to the gain at the angle of steering is reduced up to about -15 dB and -14 dB for scanning towards 30 and 45 degrees off-broadside, respectively.**

***Index Terms*—array synthesis, dual-mode antenna, grating lobes, large element spacing, Particle Swarm Optimization.**

I. Introduction

Array layouts with relatively large inter-element spacings (i.e. larger than half-wavelength at the operating frequency) can provide increased beam resolution, create more physical space for the beamformer electronics, and even relax the complexity of thermal management [1]–[3]. Due to their appealing features, such arrays have become more attractive in the recent years for various communication and sensing applications [4]–[6].

An important well-known issue in arrays with large element spacing is the possible formation of undesired grating lobes within the angular region of interest. A smart way to avoid the grating lobes is to break the periodicity in the array layout, which leads to the concept of irregular arrays [7], [8]. However, despite being very effective in dissolving the high side lobes and grating lobes, physically aperiodic arrays suffer from complex feeding structures and calibration requirements [9]. An interesting alternative to physical aperiodicity is the virtual aperiodicity, for which electronic reconfigurability is achieved at the element level so as to control the element phase centers and radiation patterns [10].

To this aim, multi-port microstrip rectangular [11] or circular [12], [13] patch antennas have been widely studied for generating multiple different resonant modes. By exciting multiple modes simultaneously, element reconfigurability is realized. The relative amplitude and phase excitations of the modes determine the phase center, radiation pattern shape and polarization properties of the element [14]. A dual-mode version of such elements were lately used for grating lobe reduction in [15], yet only with a constant phase shift between the two modes and a common amplitude ratio at the two ports found via an extensive search routine. Very recently, optimization of excitation coefficients in multi-mode antennas was proposed by exploiting a Linear Programming (LP) based approach [16], [17]. Although LP can be efficiently used in the solution of the optimization problem, it inherently limits the design constraints that can be applied during optimization. One of these constraints is on the excitation amplitudes at the element level. LP does not provide any control on the amplitudes, which leads to amplitude tapering with variable gain amplifiers and power inefficiency. On the other hand, for optimal efficiency and practical operation, it is desired that all amplifiers work at the same working point [18].

The major aim of this contribution is to study the optimization performance with the novel constraint on equi-amplitude excitations at the multi-mode array elements. For a sample analog implementation, Fig. 1(a) shows a conventional phased array configuration, while Fig. 1(b) shows the proposed beamforming scheme with dual-mode circular patch elements. The amplifiers provide fixed gain. The couplers divide the power

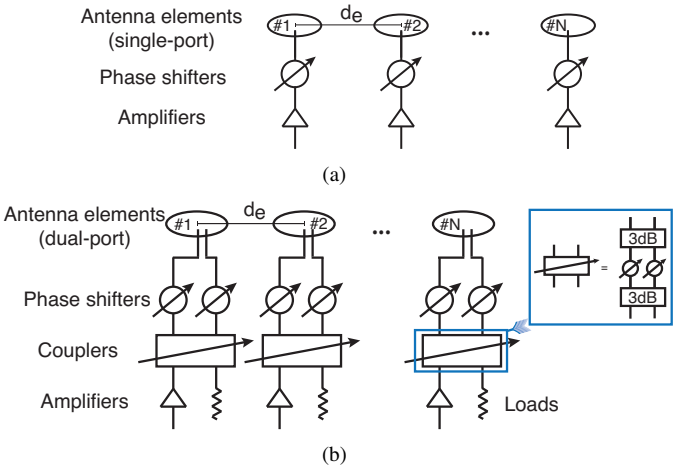

Fig. 1. Phased array architectures with equi-amplitude elements: (a) conventional topology with single mode antennas, (b) proposed topology with dual-mode antennas, d_e: inter-element spacing.

unequally, for which the variable coupling function can be achieved by two fixed back-to-back 3dB couplers with variable phase shifters in between. Note that the transmit power is identical in the two cases, yet the implementation technology specific insertion losses of the additional components should be considered in the proposed architecture in practice.

In this paper, an original array excitation coefficient optimization routine based on the configuration in Fig. 1(b) is proposed and solved by using the Particle Swarm Optimization (PSO) technique [19]. By taking the topology in Fig. 1(a) as a benchmark, the effectiveness of the method in suppressing the radiation outside the main lobe and maintaining the peak gain at the given steering angle is studied. A novel investigation on the impact of different maximal mode excitation amplitude ratios on the pattern characteristics is also performed.

The rest of the paper is organized as follows. The formulation of the array optimization problem is described in Section II. The proposed solution strategy is explained in Section III. The simulation settings and results are discussed in Section IV. The conclusions are provided in Section V.

II. Problem Formulation

The total co-polarized electric far-field at a single frequency for a scanned beam s, $f^s(\theta)$, generated by the array of dual-mode, dual-port stacked circular patch elements [14] arranged as in Fig. 2 is computed as

$$f^s(\theta) = \sum_{n=1}^{N} \left(e_{n,1}(\theta)\ w_n^s + e_{n,2}(\theta)\ q_n^s\right) \tag{1}$$

where $e_{n,1}(\theta)$ and $e_{n,2}(\theta)$ represent the complex, horizontally-polarized (according to the Ludwig-3 definition) embedded electric far-fields of the n-th element (with the origin of far-field at the center of the array) for excitation from the first (TM_{11}) port and the second (TM_{21}) port of the element, respectively. The parameters w_n^s and q_n^s denote the complex excitation weights of the n-th element for the s-th scanned beam for the first and second ports, respectively. Referring to Fig. 1(b), the aforementioned parameters can be found as

$$w_n^s = \cos(\alpha_n^s)\exp\{j\angle w_n^s\}\ ,\ q_n^s = \sin(\alpha_n^s)\exp\{j\angle q_n^s\} \tag{2}$$

where α_n^s is the coupling angle of the n-th element coupler, and $\angle w_n^s$ and $\angle q_n^s$ are the phase angles of the corresponding excitation coefficients, in radians.

In this work, we aim to optimize the values of w_n^s and q_n^s under novel design constraints so as to minimize the peak gain outside the pre-defined main lobe angular width. The first logical step is to define the set of observation angles, $\boldsymbol{\theta}_c^s$, which is an array that includes the θ angles outside the main lobe of

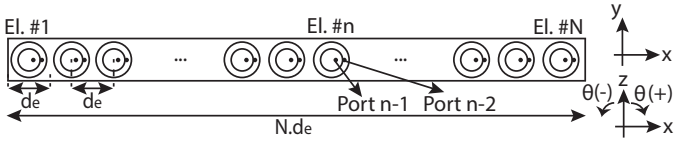

Fig. 2. Top view of the N-element linear array composed of the $d_e \times d_e$ unit cells of dual-mode elements, d_e: inter-element spacing.

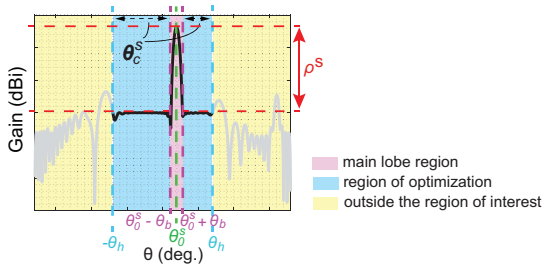

Fig. 3. Illustration of the radiation pattern related optimization parameters.

a scanned beam s. For the user inputs on the main lobe width (assumed to be constant in this work), θ_b, and the angle of steering for the s-th beam, θ_0^s, this array is expressed as

$$\theta \in \boldsymbol{\theta}_c^s \text{ if } [-\theta_h \le \theta < (\theta_0^s - \theta_b)] \text{ or } [\theta_h \ge \theta > (\theta_0^s + \theta_b)] \tag{3}$$

where θ_h limits the angular region of interest. Fig. 3 shows the radiation pattern related optimization parameters with a sample pattern shape. The optimization output ρ^s (in dB) represents the ratio of the gain at θ_0^s to the peak gain within the region of optimization observed outside the main lobe for the beam s.

Then, the overall optimization problem for our aims can be formulated for a scanned beam s as

$$\text{min. } (-\rho^s),\ \text{s.t. } \begin{cases} (|f^s(\theta_0^s)|/|f^s(\theta)|) \ge 10^{(\rho^s/20)}\ ,\ \forall \theta \in \boldsymbol{\theta_c^s} \\ |w_n^s|^2 + |q_n^s|^2 = 1,\ \forall n \in [1,\cdots,N] \\ (|q_n^s|/|w_n^s|) \le \mu,\ \forall n \in [1,\cdots,N] \end{cases} \tag{4}$$

In this formulation, the first inequality is used to define ρ^s. The second equality provides uniform-amplitude element excitations. The last condition with the user-defined input parameter μ is used to define the maximal ratio of excitation between the TM_{11} mode and the TM_{21} mode, and to analyze the pattern results for different values of μ.

III. Optimization Strategy

To solve the optimization problem formulated in (4), the Particle Swarm Optimization (PSO) technique can be effectively used. In the PSO, a candidate solution for a given non-linear problem is called a particle and K_{sw} number of particles form a swarm which is a solution space of the problem. Each particle in the swarm consists of an $N-$dimensional position vector, $X_k = (x_{k,1}, ..., x_{k,N})$, and a velocity vector of the corresponding position, $V_k = (v_{k,1}, ..., v_{k,N})$ for $k = 1, ..., K_{\text{sw}}$.

In every iteration, the position vectors are scored by a cost (fitness) function to find the fittest particle in the swarm so called personal best, p_{best}. The p_{best} becomes the global best, g_{best}, if the p_{best} of the current iteration provides a lower cost than the fittest particle that was found in the previous iterations. The position vector of the particles moves to new positions by their velocity vector. The velocity vector is updated in each iteration by the past and present experience of the particle [19]:

$$V_k^{i+1} = w_v V_k^i + c_1 r_1 (p_{best} - X_k^i) + c_2 r_2 (g_{best} - X_k^i) \tag{5}$$

where w_v is the inertial weight, c_i is the acceleration constant and r_i is the independent random number for $i = 1, 2$. The new position of the particle is found by its updated velocity given in (5) and a defined time step, Δt [19]:

$$X_k^{i+1} = X_k^i + V_k^{i+1} \cdot \Delta t \tag{6}$$

To remain in the solution space, the velocity and position of the particles are constraint to a maximum value. The velocity can be limited by a chosen maximum velocity, $v_{\max}$ [20]:

$$\text{if} \quad (|v_{\text{new}}| > v_{\max}), \qquad \text{then} \quad v_{\text{new}} = \frac{v_{\max}}{|v_{\text{new}}|} v_{\text{new}} \tag{7}$$

As for the position, the reflecting wall model has been proven to be an effective method [21]:

$$\begin{aligned} &\text{if} \quad x_{k,n} \notin [x_{n,\min}, x_{n,\max}], \qquad \text{then} \\ &x_{k,n} = 2x_{n,\min} - x_{k,n} \text{ or } x_{k,n} = 2x_{n,\max} - x_{k,n} \\ &v_{k,n} = -v_{k,n} \end{aligned} \tag{8}$$

in which the minimum and maximum positions are limited by the $x_{n,\min}$ and $x_{n,\max}$, respectively.

For the considered problem, the coupling and phase angles of the excitation coefficients are optimized. Therefore, the position vector of a particle is an N-by-3 matrix comprising α_n^s, $\angle w_n^s$ and $\angle q_n^s$ for $n = 1, ..., N$.

IV. Simulation Settings and Results

A. Single Element

A dual-mode stacked circular patch element at 9 GHz is used for demonstration purposes in our work. The element with its design parameters is shown in Fig. 4. The values of the parameters are listed in Table I. The resulting S-parameters and element patterns for the excitation of the two modes are provided in Fig. 5 for validation. As expected, the TM_{11} mode gives a beam at broadside, while the TM_{21} mode has a null at broadside at the resonant frequency of 9 GHz.

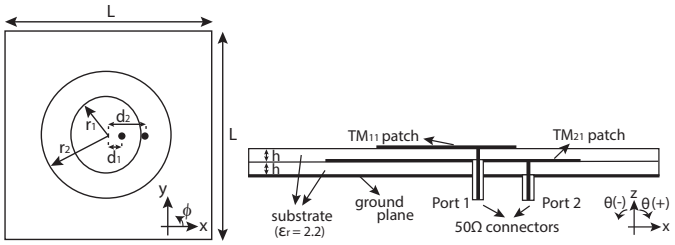

(a) (b)

Fig. 4. Dual-mode element in a unit cell: (a) top view, (b) side view.

TABLE I
VALUES OF ELEMENT DESIGN PARAMETERS

Design parameter	Value	Design parameter	Value
f_0	9.0 GHz	r_1	6.1 mm
r_2	10.1 mm	d_1	2.1 mm
d_2	6.0 mm	L	23.3 mm ($0.7\lambda_0$)
h	1.0 mm	d_e	23.3 mm ($0.7\lambda_0$)

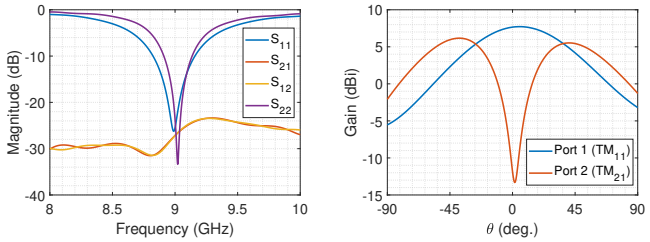

(a) (b)

Fig. 5. Full-wave simulation results of the dual-mode dual-port element in the unit cell: (a) matching and port coupling, (b) realized gain pattern at the ϕ = 0 cut for horizontal (co-) polarization for excitation at each port.

B. Benchmark Array

As a benchmark array in this work (see Fig. 2), N = 16 is used with an array having a relatively large inter-element spacing of $d_e = 0.7\lambda_0$ for f_0 = 9 GHz. The embedded element patterns at the resonant frequency are plotted in Fig. 6 for horizontal polarization for excitation of each port. For the

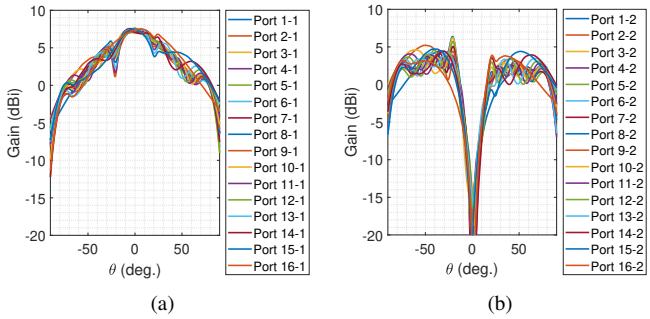

(a) (b)

Fig. 6. Embedded element realized gains for horizontal polarization in the 16-element linear array at 9 GHz for the excitation of: (a) first port (TM_{11} mode) at each element, (b) second port (TM_{21} mode) at each element.

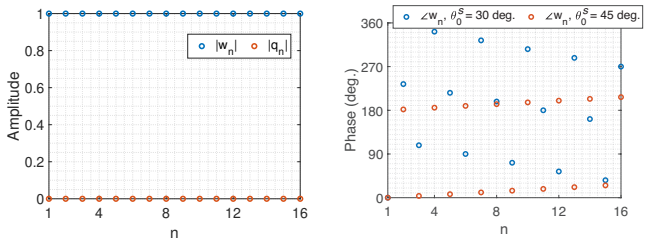

(a) (b)

Fig. 7. Excitation coefficients for the single-mode benchmark array with θ_0^s = {30,45} degrees: (a) amplitudes, (b) phases.

TABLE II
OPTIMIZATION SETTINGS

Parameter	Value	Parameter	Value
(c_1, c_2)	(2, 1)	K_{sw}	30
$(v_{\alpha,max}, v_{\phi,max})$	(0.75, 0.5)	Iteration	4000
w_v	0.2	Realization	50
Δt	0.5	(θ_h, θ_b)	$(90°, 8°)$
(r_1, r_2)	$\sim U(0, 1)$	μ	$(0.5, 1, 2)$

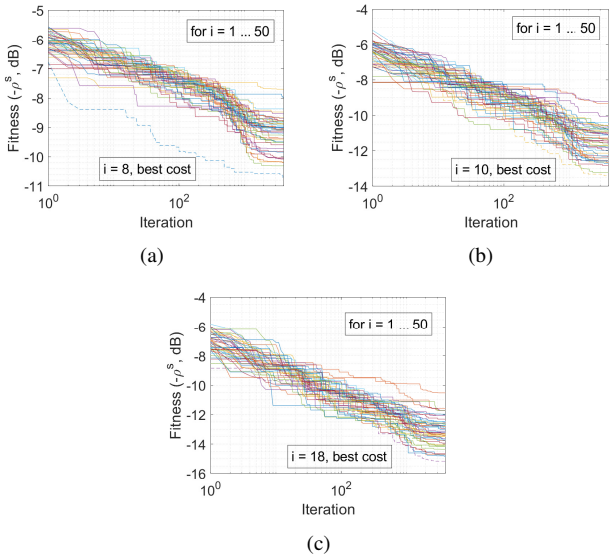

Fig. 8. Evolution of the cost function and convergence in PSO for θ_0^s = 30 degrees: (a) μ = 0.5, (b) μ = 1, (c) μ = 2.

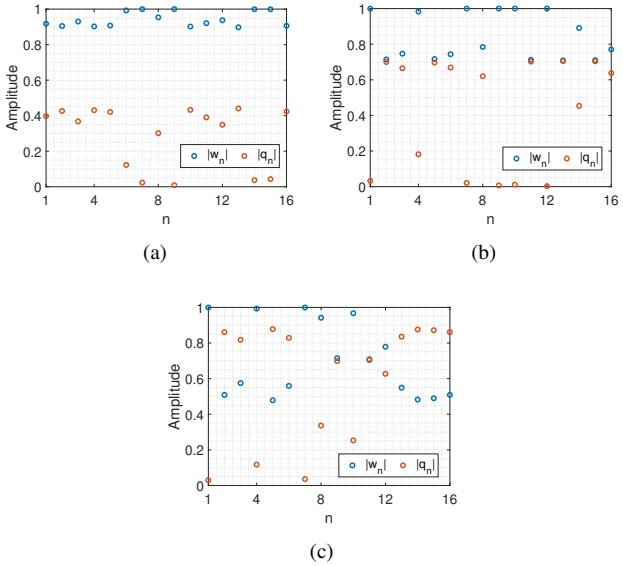

Fig. 9. Optimized excitation amplitudes for θ_0^s = 30 degrees: (a) μ = 0.5, (b) μ = 1, (c) μ = 2.

benchmark array, there is only single (fundamental, TM_{11}) mode excitation at each element with equi-amplitudes. In other words, $|w_n| = 1$, $|q_n| = 0$, $\forall n$. A progressive phase shift is applied for beam steering. In our work, we use $s = 2$ scan positions: 30 degrees and 45 degrees. The excitation amplitudes and phases for the benchmark are shown in Fig. 7. The corresponding array gain patterns with the formation of grating lobes are shown later in Fig. 11(a). The gain for 30 degree scan is computed as 17.1 dBi, while the grating lobe is 5.2 dB lower. For 45 degree scan, the gain becomes 15.1 dBi, while the grating lobe is only 0.6 dB lower.

C. Optimized Array

The optimization settings are listed in Table II. The weights in the PSO were adjusted by observing the convergence behavior of the current problem and following the common literature [20], [22]. Further, r_1 and r_2 are randomly generated numbers from the uniform distribution on the $(0, 1)$ interval. The maximum velocities of the coupling angle and phase angles are limited by the $v_{\alpha,max}$ and $v_{\phi,max}$, respectively. The swarm size was chosen as 30 and the optimizer ran 50 realizations with 4000 iterations for each array type and scanning angle. During the initialization process, the α_n^s and $\angle q_n^s$ are generated randomly. The $\angle w_n^s$ is generated by introducing randomness to the pre-calculated phase angles of the first port for the s-th scanned beam.

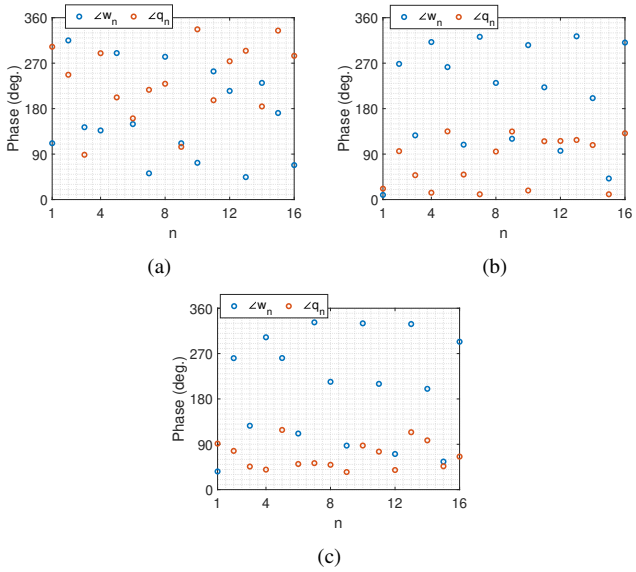

Fig. 10. Optimized excitation phases for θ_0^s = 30 degrees: (a) μ = 0.5, (b) μ = 1, (c) μ = 2.

The details of optimization results for θ_0^s = 30 degrees are given in the paper for validation. For θ_0^s = 45 degrees, only the gain patterns are included for brevity. For the former case, the evolution of the cost function and its convergence for different values of μ is shown in Fig. 8. It can be seen that for μ = 0.5, 1, 2, -ρ^s reduces to -10.7 dB, -13.4 dB and -15.2 dB, respectively. For the three values of μ, the optimized values of excitation amplitudes (satisfying the constraint $|w_n^s|^2 + |q_n^s|^2 = 1$, $\forall n$) and phases are plotted in Fig. 9 and Fig. 10, respectively. The corresponding array realized gain patterns are provided in Fig. 11(b). As compared to the benchmark, the realized gain at 30 degrees decreases by 1 dB, 0.2 dB and 1.5 dB for μ = 0.5, 1 and 2, respectively. For the latter case with θ_0^s = 45 degrees, -ρ^s reduces to -5.0 dB, -9.1 dB and -13.8 dB for μ = 0.5, 1 and 2, respectively. When compared to the benchmark array, the gain at 45 degrees is 0.8 dB larger for μ = 0.5, the same for μ = 1, and 0.8 dB smaller for μ = 2. The key radiation pattern results for the benchmark array and the optimized arrays for different values of μ are summarized in Table III for the two scan angles considered.

Lastly, it is worth to note that depending on the increased ratio of the TM_{21} mode with respect to the TM_{11} mode, the level of cross-polarization may be high at certain regions,

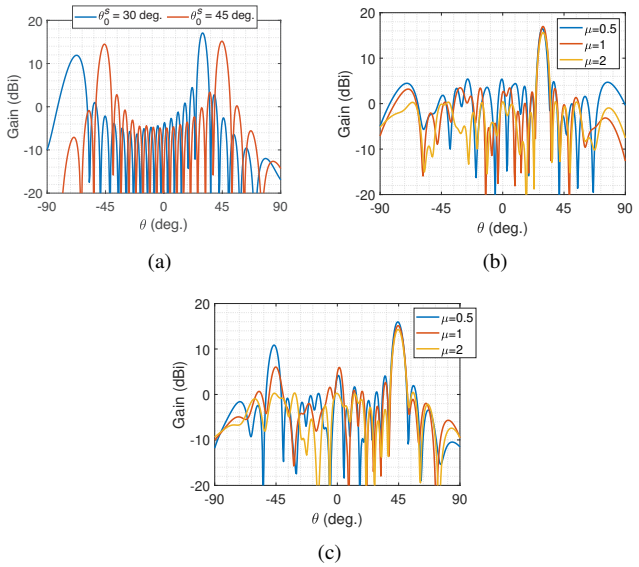

Fig. 11. Array realized gain patterns: (a) benchmark array with $\theta_0^s = \{30, 45\}$ degrees, (b) optimized array for $\theta_0^s = 30$ degrees, (c) optimized array for $\theta_0^s = 45$ degrees.

TABLE III
COMPARISON OF KEY PATTERN RESULTS FOR DIFFERENT ARRAY TYPES

Array type	θ_0^s = 30 deg.		θ_0^s = 45 deg.	
	$-\rho^s$ (dB)	Gain at θ_0^s (dBi)	$-\rho^s$ (dB)	Gain at θ_0^s (dBi)
Benchmark, μ = 0	-5.2	17.1	-0.6	15.1
Optimized, μ = 0.5	-10.7	16.1	-5.0	15.9
Optimized, μ = 1	-13.4	16.9	-9.1	15.1
Optimized, μ = 2	-15.2	15.6	-13.8	14.3

which has not been analyzed in this paper. One way to reduce the cross-polarization level is to modify the antenna structure and to add TM_{02} mode excitation [14]. However, the scope of this paper is limited to dual-mode excitation and optimization.

V. CONCLUSION

The grating lobe problem in periodic linear arrays has been addressed by employing dual-mode patch antennas. An original optimization problem has been formulated, and tailored to a novel beamforming architecture providing equi-amplitude excitations at the element level for optimal power efficiency. The PSO technique has been used to solve the problem for different upper-bounds on the ratio of excitation amplitudes of the two modes. The algorithm performance has been demonstrated by using a 16-element 0.7-wavelength spaced array of dual-port stacked patches for scanning towards 30 degrees and 45 degrees off-broadside. It has been observed that by restricting the excitation of the high order mode to a sufficiently large value, the ratio of the peak gain outside the main lobe to the gain at the angle of steering is reduced up to about -15 dB and -14 dB for scanning towards 30 and 45 degrees off-broadside, respectively. The gain reduction at the steering angle becomes no more than 1.5 dB as compared to the benchmark uniformly-fed single-mode patch array.

The study can be straightforwardly extended with the inclusion of implementation technology specific insertion losses in the proposed architecture, further investigations with multi-mode antennas, different element spacings, number of elements, scan angles and fields-of-view.

REFERENCES

[1] Y. Aslan, A. Roederer, and A. Yarovoy, "System advantages of using large scale aperiodic array topologies in future mm-wave 5G/6G base stations: an interdisciplinary look," *IEEE Syst. J.*, early access, Jan. 2021.

[2] P. Rocca, G. Oliveri, R. J. Mailloux and A. Massa, "Unconventional phased array architectures and design methodologies—a review," *Proc. IEEE*, vol. 104, no. 3, pp. 544–560, Mar. 2016.

[3] Y. Aslan, J. Puskely, J. H. J. Janssen, M. Geurts, A. Roederer and A. Yarovoy, "Thermal-aware synthesis of 5G base station antenna arrays: an overview and a sparsity-based approach," *IEEE Access*, vol. 6, pp. 58868-58882, Oct. 2018.

[4] D. Pinchera, M. D. Migliore, F. Schettino, and G. Panariello, "Antenna arrays for line-of-sight massive MIMO: half wavelength is not enough," *Electronics*, vol. 6, no. 3, p. 57, Aug. 2017.

[5] D. Pinchera, M. D. Migliore and F. Schettino, "Optimizing antenna arrays for spatial multiplexing: towards 6G systems," *IEEE Access*, vol. 9, pp. 53276-53291, Apr. 2021.

[6] S. Shakeri, D. D. Arianananda, and G. Leus, "Direction of arrival estimation using sparse ruler array design," in *Proc. 13th IEEE SPAWC*, Cesme, Turkey, Jun. 2012, pp. 525–529.

[7] M. C. Vigano, G. Toso, G. Caille, C. Mangenot, and I. E. Lager, "Sunflower array antenna with adjustable density taper," *Int. J. Antennas Propag.*, vol. 2009, pp. 1-10, Apr. 2009.

[8] Y. Aslan, J. Puskely, A. Roederer, and A. Yarovoy, "Multiple beam synthesis of passively cooled 5G planar arrays using convex optimization," *IEEE Trans. Antennas Propag.*, vol. 68, no. 5, pp. 3557–3566, Dec. 2019.

[9] M. B. Camps, "Design of a sparse irregular array for beyond 5G base stations," Master's thesis, Delft University of Technology, Delft, The Netherlands, Jul. 2021.

[10] T. Mitha and M. Pour, "Principles of adaptive element spacing in linear array antennas," *Nature Sci. Rep.*, vol. 11, no. 1, pp. 1–11, Mar. 2021.

[11] A. Narbudowicz and M. J. Ammann, "Low-cost multimode patch antenna for dual MIMO and enhanced localization use," *IEEE Trans. Antennas Propag.*, vol. 66, no. 1, pp. 405–408, Jan. 2018.

[12] E. R. Iglesias, O. Q. Teruel, and M. S. Ferfliflдez, "Compact multimode patch antennas for MIMO applications," *IEEE Antennas Propag. Mag.*, vol. 50, no. 2, pp. 197–205, Apr. 2008.

[13] T. Q. Tran and S. K. Sharma, "Radiation characteristics of a multimode concentric circular patch antenna by controlling amplitude and phase of modes," *IEEE Trans. Antennas Propag.*, vol. 60, no. 3, pp. 1601–1605, Mar. 2012.

[14] Z. Allahgholi Pour, "Control of phase centre and polarization in circular microstrip antennas," Master's thesis, The University of Manitoba, Manitoba, Canada, Jul. 2006.

[15] Z. Iqbal and M. Pour, "Grating lobe reduction in scanning phased array antennas with large element spacing," *IEEE Trans. Antennas Propag.*, vol. 66, no. 12, pp. 6965–6974, Dec. 2018.

[16] D. Inserra, F. Xie, Z. Yang, Y. Huang, J. Li, and G. Wen, "Dual-mode microstrip patch antennas for largely spaced phased arrays," in *Proc. IEEE CSRSWTC*, Fuzhou, China, Dec. 2020.

[17] Y. Aslan, "Optimization of virtually-aperiodic linear sparse arrays," *Microw. Opt. Technol. Lett.*, vol. 64, no. 2, pp. 318-324, Feb. 2022.

[18] G. Toso, P. Angeletti and C. Mangenot, "A comparison of density and amplitude tapering for transmit active arrays," in *Proc. 3rd EuCAP*, pp. 840-843, Berlin, Germany, Mar. 2009.

[19] R. Eberhart and J. Kennedy "A new optimizer using particle swarm theory," in *Proc. MHS'95*, pp. 39-43, 1995.

[20] T. M. Blackwell and P. Bentley, "Improvised music with swarms," in *Proc. CEC'02*, pp. 1462-1467, 2002.

[21] J. Robinson and Y. Rahmat-Samii, "Particle swarm optimization in electromagnetics," *IEEE Trans. Antennas Propag.*, vol. 52, no. 2, pp. 397-407, Feb. 2004.

[22] D. W. Boeringer and D. H. Werner, "Particle swarm optimization versus genetic algorithms for phased array synthesis," *IEEE Trans. Antennas Propag.*, vol. 52, no. 3, pp. 771-779, Mar. 2004.